Emission from oxygen atoms produced by electron-impact dissociative excitation of oxygen molecules

M. Bruce Schulman, Francis A. Sharpton, Sunggi Chung, Chun C. Lin, and L. W. Anderson
Department of Physics, University of Wisconsin, Madison, Wisconsin 53706
(Received 11 March 1985; revised manuscript received 11 July 1985)

Absolute optical-emission cross sections have been measured for transitions in the wavelength range 3690—11 300 Å originating from 32 terms of excited oxygen atoms produced by electron impact on oxygen molecules with incident electron energy up to 500 eV. The excitation functions show a broad peak at about 90 eV with a shoulderlike structure of varying degree near 35 eV. The observed threshold energy is very close to the energy defect of the dissociation process. Near the threshold, dissociative excitation through partly bound Rydberg states of the oxygen molecule is believed to be a major mechanism for producing the observed atomic-oxygen emission, whereas simultaneous ionization and excitation followed by dissociation become important at energies above 50 eV. Combination of the measured cross sections with theoretical transition probabilities allows us to determine the absolute optical-emission cross sections for a series of atomic-oxygen transitions in the long-wavelength infrared region of the spectrum.

I. INTRODUCTION

Excitation of bound electronic states of diatomic molecules by electron impact has been a subject of interest for many years. A closely related process is the excitation to repulsive electronic states (or partly repulsive electronic states) resulting in dissociation. While cross-section measurements for electron-impact excitation of bound electronic states of diatomic molecules have been reported from numerous laboratories, similar experiments for dissociative excitation are comparatively scarce. In addition to its intrinsic interest as a fundamental collisional process, electron-impact dissociative excitation furnishes a mechanism for producing excited atoms and the emission associated with them.[1]

An earlier paper by Filippelli *et al.*[2] reports the production of excited N atoms by electron-impact dissociative excitation of N_2; the optical method was employed to investigate atomic transitions in the range 3830 —10 600 Å. In the present work we extend the electron-impact dissociative excitation experiment to O_2 in the $X^3\Sigma_g^-$ ground state. We present here measurement of optical-emission cross sections for transitions originating from 32 terms of atomic oxygen (O I), corresponding to eighteen of the $2p^3nl$ excited configurations. We also investigate the dissociation process by applying previously calculated O_2^+ potential-energy curves[3] to the analysis of our measured threshold incident electron energies for production of several excited atomic states. By using theoretical transition probabilities we deduce optical-emission cross sections for a series of long-wavelength infrared lines emitted by these excited oxygen atoms.

Most investigations of electron-impact dissociative excitation of O_2 have involved detection of vacuum-ultraviolet (vuv) emission; atomic transitions in the range 862—1358 Å have been reported.[4—13] Previous studies of emission at longer wavelengths have been more limited.[4,11,14,15] Our present work in the near-ultraviolet to infrared spectral range together with the earlier experiments furnish a comprehensive study of the emissions from excited oxygen atoms produced by electron impact on O_2 molecules.

II. EXPERIMENTAL

In our experiment, a collimated monoenergetic electron beam is generated by an electron gun in a collision chamber which has been evacuated to a pressure of 3×10^{-6} Torr and then filled with research-grade oxygen gas at a pressure below 25 mTorr. Production of excited oxygen atoms by electron-impact dissociation of O_2 molecules is studied by observing the optical radiation that is emitted perpendicular to the beam. A schematic diagram of the apparatus is shown in Fig. 1. The light emerging from a small volume of space in the Faraday cup is focused with unit magnification onto the entrance slit of the monochromator. The dispersed emission lines are detected by analyzing the photomultiplier-tube (PMT) output current.

The electron gun and optical system have been described in detail.[2] The electron source is a thoria-coated V-shaped iridium filament.[16] The gas pressure in the working range 1—25 mTorr is measured with a MKS Baratron model 220B capacitance manometer. For the range 3690—8820 Å, a RCA C31034 PMT cooled to −15 °C was used; for the range 8446—11 300 Å, a RCA 7102 PMT cooled to −60 °C was used. To permit the determination of absolute optical-emission cross sections, an absolutely calibrated GE type-20A/T24/2 tungsten-ribbon radiance source (RS) was optically substituted for the electron-beam-excited source (see next paragraph). Colored filters were used when studying wavelengths longer than 6500 Å. The equipment used for obtaining optical excitation functions consists of an ORTEC series 9300 photoelectron-pulse counting system. The electron beam is switched on and off by modulating the control-

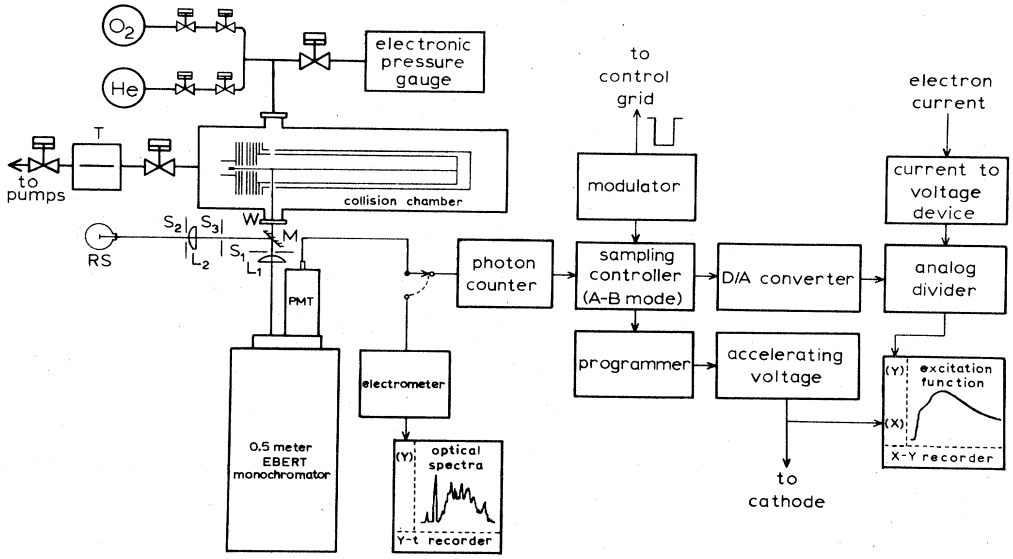

FIG. 1. Schematic diagram of experimental apparatus. T, concentric-cylinder-type liquid-nitrogen-cooled trap; W, 3.2-mm-thick uv-grade fused-silica window; S_1 and S_2, circular aperture stops; S_3, field stop imaged onto the monochromator entrance slit with unit magnification; L_1 and L_2, achromatic lenses. Other components are described in the text. The electron gun is shown to scale.

grid voltage at a rate of 50 Hz. This allows subtraction of the signal due to scattered filament light and PMT dark current. For lines with high signal-to-noise ratio, excitation functions were also measured with the Keithley model 610B electrometer substituted for the ORTEC system.

The optical-emission cross section $Q_{\text{opt}}(i\rightarrow j)$ of a radiative transition was calculated by the method described by Sharpton *et al.*[17] We use the formula

$$Q_{\text{opt}}(i\rightarrow j)=\frac{|e|}{\rho L I_e}\left[4\pi A_s F(\lambda,T)\Delta\lambda\frac{\Omega_s\gamma_s(\lambda)R_c}{\Omega_c\gamma_c(\lambda)R_s}\right], \tag{1}$$

where I_e is the electron current, e is the electron charge, ρ is the gas number density, and L is the length of the electron beam viewed by the monochromator. The expression in large parentheses is the entire photon flux collected per second from the $i\rightarrow j$ atomic-oxygen emission; the subscripts c and s refer to the collision chamber and standard lamp sources, respectively. A_s is the effective radiation area of the standard lamp, Ω is the solid angle of observation, $\gamma(\lambda)$ is the transmittance at the wavelength λ of the light path, and R is the PMT signal measured with the electrometer (background and dark current subtracted). The quantity $F(\lambda,T)\Delta\lambda$ is the rate of emission of photons,[18] emitted in the range λ to $\lambda+\Delta\lambda$ by the standard lamp operating at an absolute temperature T, which are transmitted by the monochromator with a passband $\Delta\lambda$. In the earlier work by Filippelli *et al.*,[2] the standard lamp was positioned behind the collision chamber and on the optical axis from the monochromator entrance slit to the source region in the Faraday cup. Because of later alterations in the vacuum system, it was necessary for us to operate the standard lamp at a right angle to the original axis by introducing the plane mirror M. To elminate the uncertainties introduced by partial polarization of the standard-lamp light by reflection from the mirror, the response of the detection system to that source was measured for both configurations (through the collision chamber and through the mirror). From these data the correction for the change in response due to polarization introduced by the mirror was obtained, and this is included in our transmittance function $\gamma_s(\lambda)$.

The gas number density was determined by measuring the pressure p with the Baratron gauge and then applying the ideal-gas equation. Departure of the gas density in the Faraday cup from this value was studied using the benchmark optical cross sections for electron-impact production of $n\ ^1S\rightarrow 2\ ^1P$ transitions of He ($n=3,4,5,6$) presented by Van Zyl *et al.*[19] The cross sections of these lines, with wavelengths ranging from 417 to 728 nm, were measured at 50, 100, and 500 eV incident electron energy E for $1\leq p\leq 30$ mTorr and $3\leq I_e\leq 50$ μA using Eq. (1). The cross sections of the 505- and 728-nm transitions were extrapolated to zero pressure to correct for radiation trapping. Our measured cross sections Q_m were consistently smaller than the published results Q_b of Ref. 19; we found $Q_b=Q_m/0.88$. We attribute this effect to reduction in local gas density caused by the hot filament, as described by Filippelli *et al.*[20] This constant factor was thereafter included in Eq. (1) to correct for the systematic error.

The presence of hot metal surfaces in contact with the highly reactive O_2 gas placed several constraints on the range of pressure available to us for study. When evacuating the collision chamber, the pressure could be monitored with an ionization gauge for $p<10^{-3}$ Torr. However, care was taken not to operate this gauge in a

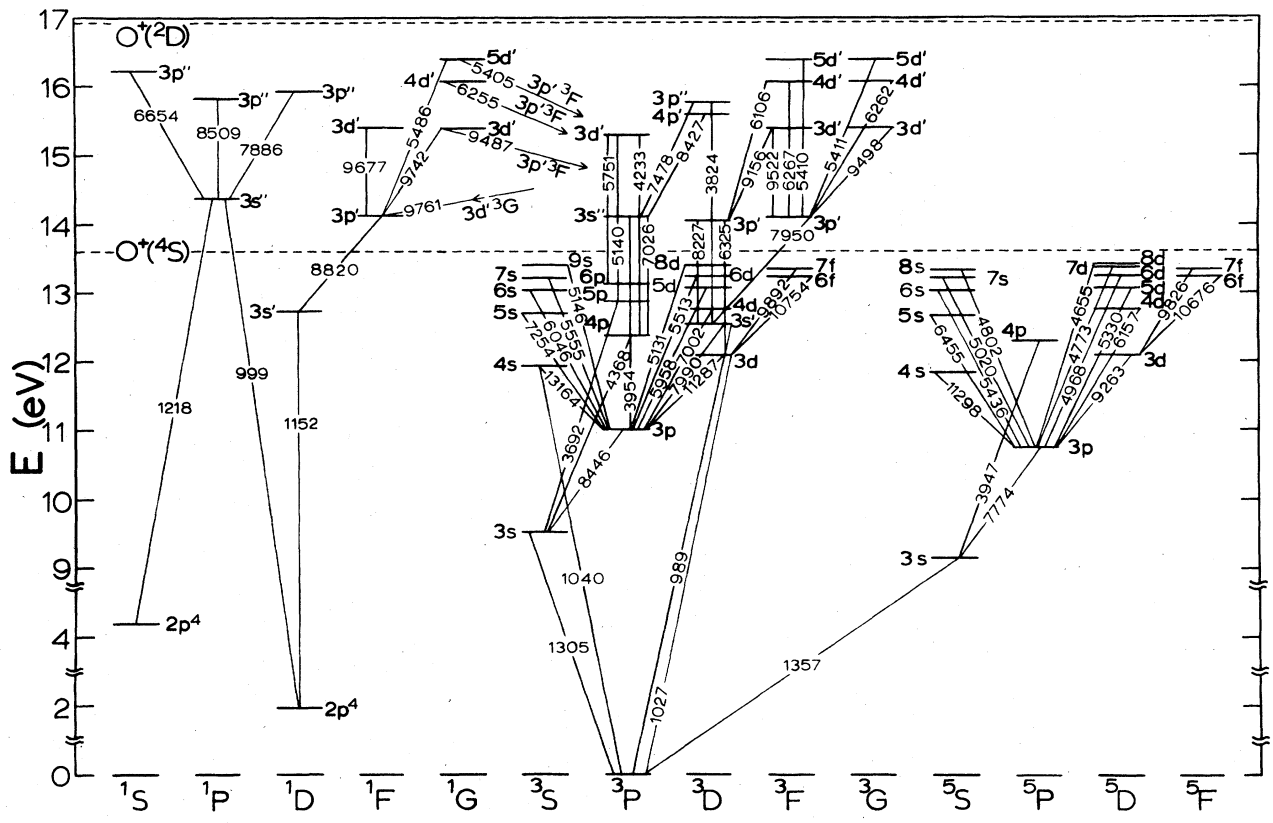

FIG. 2. Partial energy-level diagram for atomic oxygen in which all of the transitions studied in this work are shown. We also include several transitions which fall outside our range of observation, but have been studied by other researchers. Wavelengths are given in Å.

predominantly oxygen environment for $p \gtrsim 10^{-4}$ Torr because of possible damage to its hot filament. No data could be taken for $p \lesssim 10^{-5}$ Torr because contamination of the signal by atmospheric gas leaking through the "O-ring" seals became significant in this range. We were therefore limited to obtaining data with O_2 pressure in the range available to the Baratron gauge ($p \gtrsim 1$ mTorr). Likewise, the electron gun was not operated for $p > 25$ mTorr to avoid damage to the iridium filament.

Figure 2 is a partial energy-level diagram for O I based on Ref. 21, in which we indicate all the transitions studied in this work and several transitions studied by other researchers which fall outside our range of observation. In some cases, our failure to detect an emission line allowed us to place an upper limit on its optical-emission cross section. Equation (1) is valid when a single $i \rightarrow j$ transition can be resolved. For unresolved multiplets, the product $R_c \Delta\lambda$ in Eq. (1) was replaced by the appropriate integrated area under the multiplet peak as measured from the spectrum taken on the strip chart. This gives the absolute optical-emission cross section for a multiplet,

$$Q_{\text{opt}}(A \rightarrow B) = \sum_{J,J'} Q_{\text{opt}}(A_{J'} \rightarrow B_J) , \tag{2}$$

where A,B represent the initial and final terms, and J',J are the total-angular-momentum quantum numbers.

In Fig. 3 we show a typical measured spectrum. In this scan, the intensity of several weak O_2^+ bands relative to the strongest O I multiplets (7774 and 8446 Å) and two of the weaker O I multiplets (7002 and 8222–8235 Å) is apparent. The insets indicate the signal-to-noise level and problems of blending with the molecular signal. For the 7002- and 8222-Å transitions, the excitation function taken with the monochromator passband centered on the atomic line (position a in the insets of Fig. 3) contained non-negligible contamination from overlapping O_2^+ emission. In these cases a second excitation function was taken immediately after the first under the same experimental conditions, but with the monochromator passband positioned over the molecular background signal at a point about 10 Å away from the O I line (position b). The background excitation function was later subtracted from that of the combined O I and O_2^+ radiation so that an excitation function of the pure O I emission could be obtained.

To measure cross sections for production of the stronger O I multiplets, O_2 was sealed within the evacuated collision chamber at a pressure less than 12 mTorr. For the very weak lines, pressures in the range 13–18 mTorr were used, often with O_2 flowing slowly through the system to avoid collection of atmospheric gas from long-term leakage. In these cases, the PMT signal was recorded as the monochromator was first scanned across the weak line; then the monochromator was quickly tuned to a nearby strong O I line for which we had determined

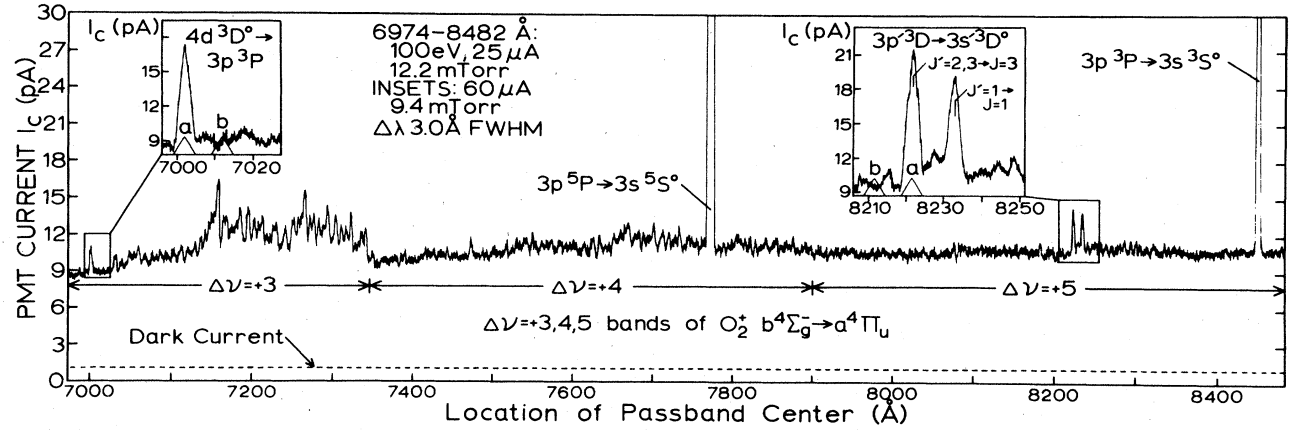

FIG. 3. Signal developed from a limited spectral scan of the emission resulting from electron-impact excitation of the O_2-gas sample. The triangular passband with $\Delta\lambda = 3$ Å full width at half maximum (FWHM) is shown in the insets of this figure.

the absolute optical cross section, and the procedure was repeated. Since the absolute calibration of the optical system and PMT signal is known, this enabled us to obtain the ratio of the two cross sections without having to accurately determine the density of the slowly flowing O_2 gas.

III. RESULTS

A. Optical-emission cross sections

Our test experiments show that the emission signal R_c is proportional to the O_2 pressure over the range 1—20 mTorr and proportional to the electron-beam current over the range 1—50 μA for the $3p\,^3P \rightarrow 3s\,^3S^0$ transition at $E = 100$ eV. Likewise, the emission signals of several highly excited transitions were found to be linear with the gas pressure in the range 1—18 mTorr at 100 eV. The experimental data for this linear regime are shown in Fig. 4(a). The data for these least-squares-fitted lines have been scaled as necessary to facilitate visual comparison. When extrapolated to zero pressure, these plots give zero signal to within the experimental uncertainty. Cross sections and excitation functions were not measured with $I_e > 50$ μA because cooling of the iridium filament by the O_2 gas made it very difficult to obtain larger beam currents. We note that Filippelli[22] found that for dissociative excitation of N_2 the signal was proportional to the current for $I_e \lesssim 250$ μA at $E \simeq 85$ eV and $p \lesssim 14$ mTorr. We therefore believe that in our experiment the linearity of signal with current is well satisfied in all cases.

For the region $E \gtrsim 110$ eV, in which the O I optical cross sections decrease with increasing E, the signal was found to depend nonlinearly on the pressure. In Fig. 4(b) the signal developed from the $3p\,^5P \rightarrow 3s\,^5S^0$ transition is shown as a function of pressure for several incident electron energies. The data for these curves have been scaled to make them all agree in slope in the low-pressure region

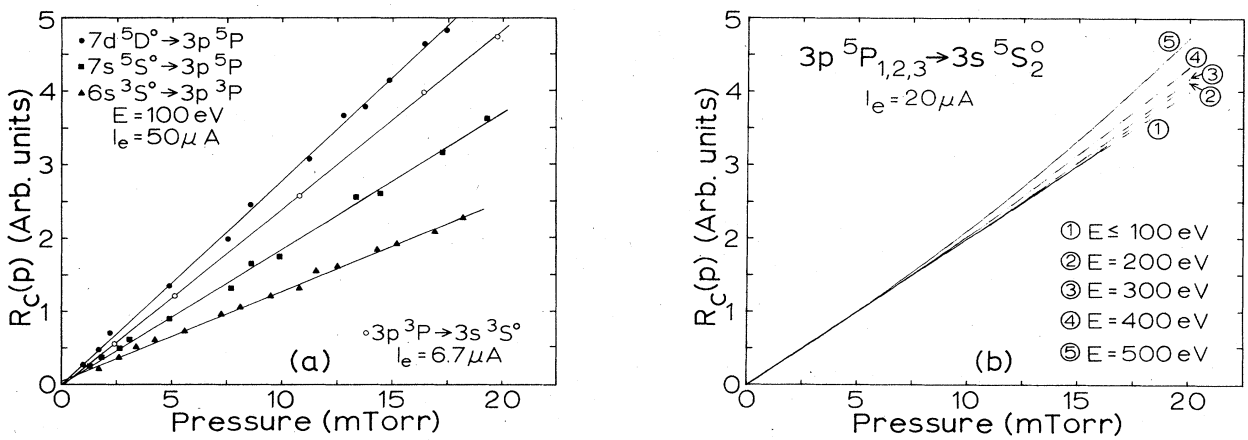

FIG. 4. (a) Illustration of the linearity with pressure in the signal from several O I multiplets, measured at an incident electron energy of 100 eV. The solid lines are least-squares linear fits to the experimental data. The vertical uncertainty in each point is approximately as large as the characters which mark the points. R_c is the PMT signal after subtraction of background and dark current. Each curve has been scaled as necessary to facilitate comparison. (b) Illustration of the nonlinearity with pressure in the $3p\,^5P \rightarrow 3s\,^5S^0$ emission signal for energies greater than 100 eV, with I_e held fixed at 20 μA. The curves have been scaled as necessary to agree in slope in the low-pressure regime. The data generally lie within a few percent of these cubic-spline-fitted curves.

TABLE I. Excitation cross sections $Q_{opt}(A \rightarrow B)$ for O emission observed in this work, as produced by dissociative electron-impact excitation of O_2. The incident electron energy is 100 eV, except where noted. Each cross section is for the sum over all $J' \rightarrow J$ components of a transition, unless otherwise specified.

O multiplet[a]	λ_{air} (Å)	$\sum_{J,J'} Q_{opt}(J' \rightarrow J)$[b] ($10^{-20}$ cm^2)
$4s\ ^5S^0 \rightarrow 3p\ ^5P$	11 295.1—11 302.4	61
$5s\ ^5S^0 \rightarrow 3p\ ^5P$	6453.6—6456.0	3.7[c]
$6s\ ^5S^0 \rightarrow 3p\ ^5P$	5435.2—5436.9	0.75[c]
$7s\ ^5S^0 \rightarrow 3p\ ^5P$	5018.8—5020.2	0.29[c]
$8s\ ^5S^0 \rightarrow 3p\ ^5P$	4801.8—4803.0	<0.17
$3p\ ^5P \rightarrow 3s\ ^5S^0$	7771.9—7775.4	430[c]
$4p\ ^5P \rightarrow 3s\ ^5S^0$	3947.3—3947.6	1.1[c,d]
$3d\ ^5D^0 \rightarrow 3p\ ^5P$	9260.8—9266.0	124[c]
$4d\ ^5D^0 \rightarrow 3p\ ^5P$	6156.0—6158.2	11[c]
$5d\ ^5D^0 \rightarrow 3p\ ^5P$	5329.1—5330.7	3.4[c]
$7d\ ^5D^0 \rightarrow 3p\ ^5P$	4772.4—4773.8	0.58
$8d\ ^5D^0 \rightarrow 3p\ ^5P$	4654.1—4655.4	0.25 (50 eV)
$6f\ ^5F \rightarrow 3d\ ^5D^0$	10 675.7—10 675.9	4.5
$7f\ ^5F \rightarrow 3d\ ^5D^0$	9825.8—9826.0	2.4
$6s\ ^3S^0 \rightarrow 3p\ ^3P$	6046.2—6046.5	0.30[c]
$7s\ ^3S^0 \rightarrow 3p\ ^3P$	5554.8—5555.0	<1.9[c]
$9s\ ^3S^0 \rightarrow 3p\ ^3P$ $3d'\ ^3P_2^0 \rightarrow 5p\ ^3P$	5146.1	<0.02[e]
$3p\ ^3P \rightarrow 3s\ ^3S^0$	8446.2—8446.8	200[c]
$4p\ ^3P \rightarrow 3s\ ^3S^0$	4368.2	2.2 (50 eV)
$5p\ ^3P \rightarrow 3s\ ^3S^0$	3692.4	0.04
$3s''\ ^3P^0 \rightarrow 3p\ ^3P$	3951.9—3954.6	<0.01 (50 eV)
$3s''\ ^3P_2^0 \rightarrow 4p\ ^3P$	7025.5	<0.10
$3d'\ ^3P_2^0 \rightarrow 4p\ ^3P$	4233.3	<0.01[e]
$3d'\ ^3P_2^0 \rightarrow 6p\ ^3P$	5750.6	<0.03[e]
$3d\ ^3D^0 \rightarrow 3p\ ^3P$	11 286.3—11 287.3	52
$3s'\ ^3D^0 \rightarrow 3p\ ^3P$	7981.9—7987.3 7995.1	<0.10
$4d\ ^3D^0 \rightarrow 3p\ ^3P$	7001.9—7002.2	1.4[c]
$5d\ ^3D^0 \rightarrow 3p\ ^3P$	5958.4—5958.6	<2.0[c]
$6d\ ^3D^0 \rightarrow 3p\ ^3P$	5512.6—5512.8	<0.25
$8d\ ^3D^0 \rightarrow 3p\ ^3P$ $3d'\ ^3P_1^0 \rightarrow 5p\ ^3P$	5130.4—5130.7	<0.03
$3p'\ ^3D \rightarrow 3d\ ^3D^0$	6323.4—6324.8	<1.1
$3p'\ ^3D \rightarrow 3s'\ ^3D^0$	8221.8 8227.7—8235.4	8.6[c,f]
$4p'\ ^3D \rightarrow 3s''\ ^3P^0$	8420.9 8424.7—8429.1	<0.65
$3p''\ ^3D \rightarrow 3s'\ ^3D^0$	3822.6—3825.5	<0.02
$3p''\ ^3D \rightarrow 3s''\ ^3P^0$	7471.4—7473.2 7476.4—7480.7	<1.1
$6f\ ^3F \rightarrow 3d\ ^3D^0$	10 753.5	3.7
$7f\ ^3F \rightarrow 3d\ ^3D^0$	9891.7	1.5
$3p'\ ^3F \rightarrow 3s'\ ^3D^0$	7952.2—7947.2 7939.5, 7943.2	<0.59
$3d'\ ^3F_4^0 \rightarrow 3p'\ ^3D_3$	9156.0	2.9
$3d'\ ^3F^0 \rightarrow 3p'\ ^3F$	9517.0—9528.6	2.0
$4d'\ ^3F^0 \rightarrow 3p'\ ^3D$	6106.3—6107.6	0.31[c]
$4d'\ ^3F_4^0 \rightarrow 3p'\ ^3F_4$	6266.9	0.29[e]
$3d'\ ^3G^0 \rightarrow 3p'\ ^3F$	9492.7—9505.6	6.8[g]

TABLE I. (*Continued*).

O multiplet[a]	λ_{air} (Å)	$\sum_{J,J'} Q_{opt}(J' \rightarrow J)$[b] ($10^{-20}$ cm^2)
$3d'\,^3G_4^0 \rightarrow 3p'\,^1F$	9760.7	2.0
$4d'\,^3G^0 \rightarrow 3p'\,^3F$	6259.2—6264.5	0.46[e,g]
$5d'\,^3G^0 \rightarrow 3p'\,^3F$ $5d'\,^3F^0 \rightarrow 3p'\,^3F$	5408.6—5414.6	0.17[c]
$3p''\,^1S \rightarrow 3s''\,^1P^0$	6653.8	<0.22[e]
$3p''\,^1P \rightarrow 3s''\,^1P^0$	8508.6	<0.08
$3p''\,^1D \rightarrow 3s''\,^1P^0$	7886.3	<0.15
$3p'\,^1F \rightarrow 3s'\,^1D^0$	8820.4	4.4
$3d'\,^1F^0 \rightarrow 3p'\,^1F$	9677.4	<0.46[e]
$3d'\,^1G^0 \rightarrow 3p'\,^1F$	9741.5	3.0
$3d'\,^1G^0 \rightarrow 3p'\,^3F$	9481.2—9487.4	4.3
$4d'\,^1G^0 \rightarrow 3p'\,^3F$	6254.1—6256.8	0.27[e]
$5d'\,^1G^0 \rightarrow 3p'\,^1F$	5486.5	<0.05
$5d'\,^1G^0 \rightarrow 3p'\,^3F$	5405.0	0.04

[a]Upper states are listed in order of energy within groups of increasing L and S, except where unrelated transitions are not resolved. A prime symbol (′) on the configuration notation indicates the corresponding state of $O^+(^2D^0)$ as core; a double-prime symbol (″) indicates $O^+(^2P^0)$ as core; otherwise, an $O^+(^4S^0)$ core.

[b]Estimated uncertainty 20%, except those with superscripts c and e. We first assign an overall minimum uncertainty of 15% to these cross sections by adding in quadrature the estimated extreme fractional error in each of the factors appearing in our cross section formula. For those values lacking the c or e superscripts, the uncertainty is increased to 20% because of low signal-to-noise ratio, or overlapping O_2^+ bands. In several cases a cross section was measured at 50 eV incident electron energy to eliminate the signal from an overlapping O^+ line.

[c]Estimated uncertainty 15%.

[d]Falls near $O^+(3p\,^2P^0_{3/2} \rightarrow 3s\,^2P_{1/2})$ at 3945 Å, and slight contamination is possible. At 50 eV the measured cross section is 0.64×10^{-20} cm$^2 \pm 15\%$.

[e]Estimated uncertainty of up to 50% because of very low signal-to-noise ratio, or contamination from overlapping O_2^+ bands.

[f]Some $J' \rightarrow J$ components of this multiplet were partially resolved and measurable. The cross section presented is the sum of the cross sections of the partially resolved components. See Table II also.

[g]$J' = 3 \rightarrow J = 4$ excluded.

where R_c is proportional to pressure. For $E = 500$ eV, the pressure dependence of R_c for this transition was found to be very well described by the form $ap + bp^2$, with $b/a \simeq 0.0140$ mTorr^{-1}. A nonlinearity of the type illustrated in Fig. 4(b) was found for all the O I transitions for which we could determine the energy dependence of the emission signal. We give more details of this effect in the discussion of our measured optical excitation functions. In this paper we are mainly interested in dissociative excitation in the linear-pressure and linear-current regime, and hence we have not performed experiments to identify the processes that are responsible for the quadratic-pressure component of the emission signal.

Based upon the available radiative lifetime data for the O I excited states studied in this work, most of them have lifetimes of 1×10^{-7} s or less.[23–25] Assuming a total center-of-mass kinetic energy as large as 5 eV for the fragment atoms (dissociation via a repulsive state), their speeds would be less than 8×10^5 cm/s in the lab, and they would travel less than 0.8 mm during their excited lifetimes. The radial extent of the emitting region was measured for the three transitions indicated in Fig. 5 by placing a slit of width $w = 0.394$ mm directly in front of and perpendicular to the monochromator entrance slit, and translating it perpendicular to the plane of Fig. 1. Assuming that the profiles are nearly Gaussian distributions, less than 1% of the signal is lost in the extreme case, and therefore this is neglected in our data analysis.

Finally, we expect that polarization of the atomic radiation is a negligible effect in our measurement of optical-emission cross sections, since the dissociation proceeds through many intermediate states. Lawrence[4] determined that the O I 8446-Å radiation produced by electron-impact dissociative excitation of CO is polarized less than 0.5%. Also, Filippelli *et al.*[2] reported less than 5% polarization for emission lines of excited N atoms produced by electron-impact dissociation of N_2. For these reasons we believe that polarization effects are of negligible importance in this work.

The O I transitions identified in this work are listed in Table I, along with our measured optical-emission excitation cross sections. In addition, we list transitions for which an upper bound to the cross section could be obtained. The uncertainty of each cross section is given and

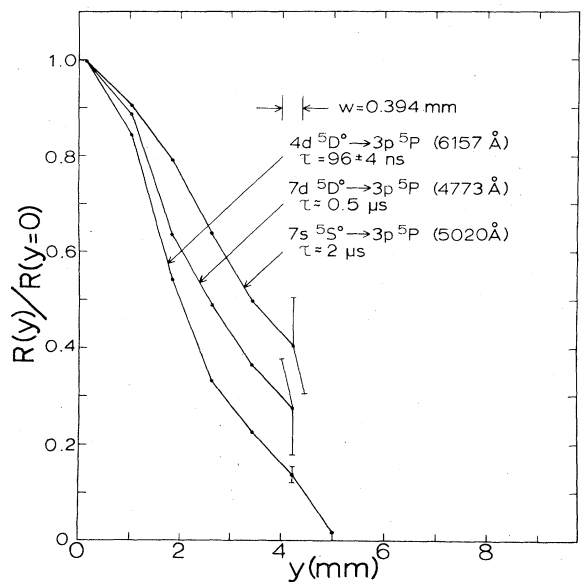

FIG. 5. Illustration of radiative lifetime effect on the spatial extent of the emitting region using as signal emission from three longer-lived O I states. The profiles were obtained at $E=100$ eV, $I_e=50\ \mu$A, and $p=13.7$ mTorr. $y(\text{mm})=Y-Y_0$, where Y is the coordinate giving the location of the center of the vertically translatable slit of width $w=0.394$ mm, and Y_0 is the slit coordinate for which the signal $R(y)$ is a maximum. $R(y)$ is the signal with background and dark current subtracted. For the $4d\ ^5D^0\rightarrow 3p\ ^5P$ transition, τ is taken from Ref. 23. For the $n'=7$ transitions, τ is an estimate based on lifetimes of lower-lying transitions of the same series given in Refs. 23 and 24.

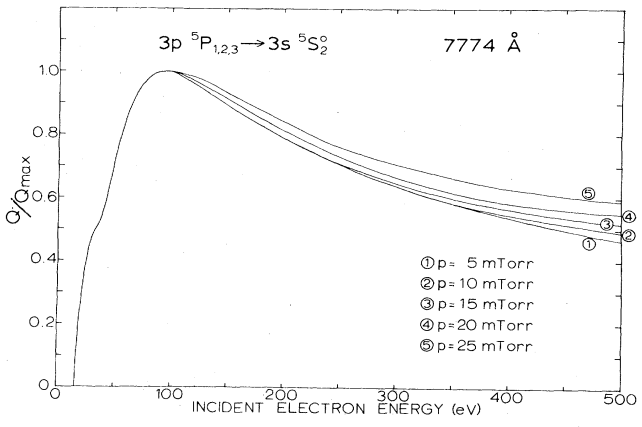

FIG. 6. Illustration of the variation with pressure in the measured excitation function of the $3p\ ^5P\rightarrow 3s\ ^5S^0$ multiplet, as a function of the incident electron energy E. In each case the electron-beam current was held fixed at 20 μA throughout the energy range. For each curve, the cross-section data have been normalized to a maximum value of 1.0. The curves are cubic-spline fits to the experimental data. For $p=5$ mTorr and $E>105$ eV the optical-emission cross-section data are well described by the form $Q_{\text{opt}}=(C_1/E)\ln(E/C_2)$, where C_1 and C_2 are constants.

explained in the footnotes of Table I. The uncertainty in the ratio of cross sections for two different lines at the same energy, or for the same line at two different energies, is considerably smaller than that obtained from the individual uncertainties. In Table II we compare our measurements with cross sections of transitions within our range reported by other researchers. The agreement is satisfactory in each case. In Table III we list additional O I transitions studied by other researchers, but falling beyond our range of observation.

B. Excitation functions

To within the sensitivity of our apparatus, the shapes of the excitation functions for energies below that of the broad maximum ($E\simeq 100$ eV) are independent of pressure within the range studied. However, the height of the decreasing "tail" region ($E\gtrsim 110$ eV) relative to the broad maximum is not independent of pressure. In Fig. 6 we show the effect of increasing pressure on the shape of the excitation function of the 7774-Å transition. As the pressure is increased beyond 5 mTorr at high electron energies, $Q_{\text{opt}}(E)$ increases relative to $Q_{\text{opt}}(E<100$ eV). As the pressure increases, the nonlinear behavior begins at lower electron energies. This effect is the result of the weak quadratic behavior of $R_c(p)$ discussed in subsection A. For $p=5$ mTorr and $105<E<500$ eV, this optical cross section has an energy dependence well described by the form $Q_{\text{opt}}=(C_1/E)\ln(E/C_2)$, where C_1 and C_2 are constants, with $C_2=29.80$ eV. The pressure dependence illustrated in Fig. 6 is typical of all the O I transitions for which we could determine excitation functions, although the strength and energy onset of the nonlinearity is different for the various transitions.

In Fig. 7 we present optical excitations functions for twelve transitions over the energy range 0—400 eV. The excitation functions of the transitions at 8820, 6046, 7002, and 6106 Å were measured at pressures of 12—15 mTorr. The data for the 8222- and 5436-Å functions were obtained at pressures of 17—18 mTorr. The remainder of the excitation functions in Fig. 7 were measured at pressures of 6—10 mTorr. In each case the O_2 gas was flowing slowly through the system. Contamination by overlapping O_2^+ emission is negligible for all the quintet transitions and for the $3p\ ^3P\rightarrow 3s\ ^3S^0$ transition. Correction for contamination by O_2^+ emission using the method described in Sec. II was necessary for the rest of the excitation functions in Fig. 7.

C. Threshold dissociative excitation

Like the case of electron-impact dissociative excitation of N_2, the threshold incident electron kinetic energy needed to produce O I emission by dissociative excitation is of special interest (see next section). The threshold incident electron energy for a transition was determined by comparing the experimental threshold accelerating voltage for the O I emission line with that for particular He or Ar lines, for which the corresponding threshold energies are

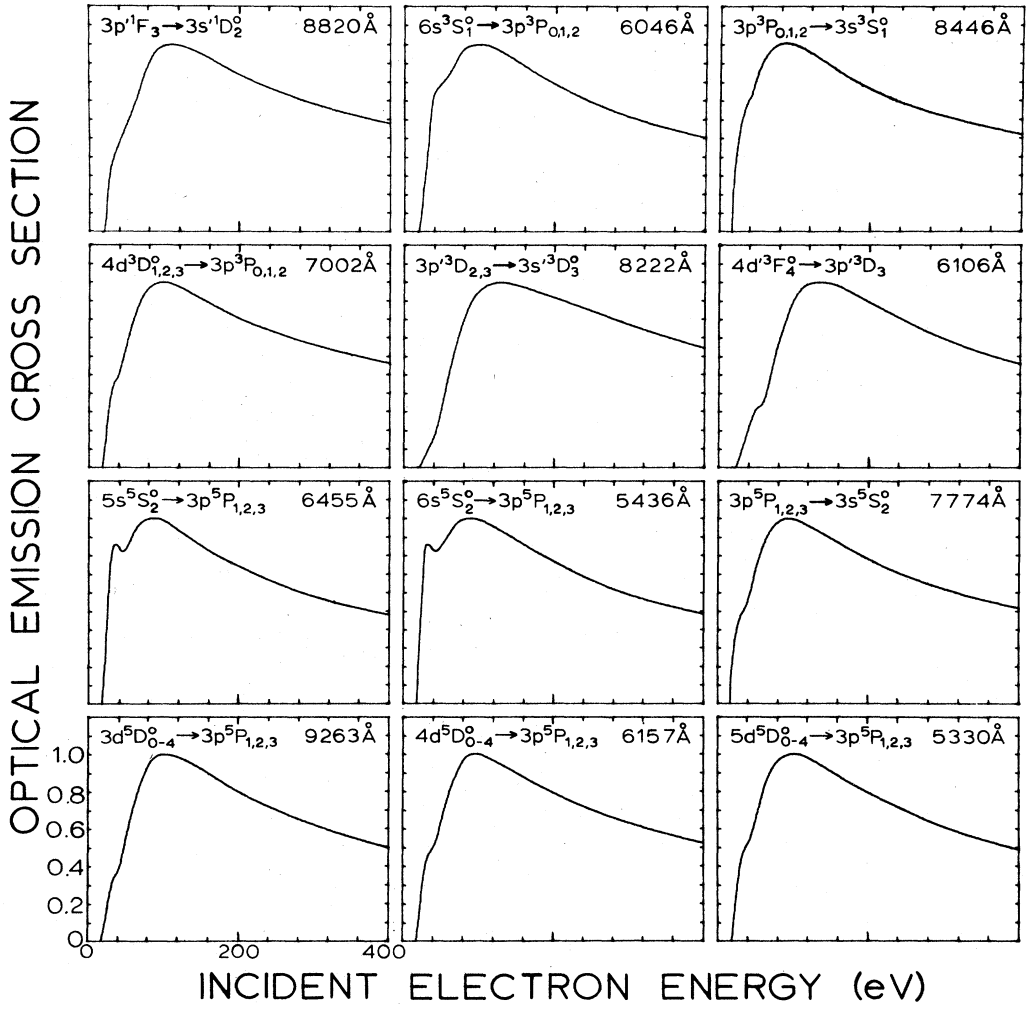

FIG. 7. Shape of optical-emission excitation functions for atomic-oxygen multiplet radiation, as determined in this work. The curves are cubic-spline fits to the experimental data, and have been normalized to a maximum value of 1.0 in each case. All curves shown here are plotted to the same energy scale. See Table I for the absolute cross-section value corresponding to 100 eV.

known.[2] For these onset measurements, O_2 was flowed slowly through the system at a pressure of about 16 mTorr along with about 4 mTorr of He or Ar, and the desired emission signals were plotted against accelerating voltage in the onset region (without division by I_e). In this short energy interval the electron-beam current is a very slowly changing function of accelerating voltage. For the 7774-Å O I multiplet the onset was also measured with I_e held fixed; the result differed from that of the variable-current method by less than the experimental uncertainty. We found that accurate threshold measurements could be obtained only if the electron beam was kept tightly focused.

Comparison transitions were chosen on the basis of proximity to an O I line in wavelength and threshold energy, with the additional requirements of high intensity and sharply increasing cross section near threshold. By measuring an O I onset energy relative to a comparison transition, we eliminate from consideration the small deviation of the true energy of the electrons from the accelerating voltage between cathode and ground. In Fig. 8 we show the experimental signal resulting from the electron-energy distribution function convoluted with the foot of the cross-section curve for two O I transitions and two comparison transitions. Each curve has been scaled and shifted vertically as necessary to facilitate visual comparison. It is seen that there is a small region of ≈ 0.5 eV over which each curve changes from zero to a steeply rising curve with linear dependence on electron energy. The width of this region indicates the total electron-energy spread in the beam. Our data are thus consistent with a full width at base of ≈ 0.5 eV for the incident electron-energy distribution at threshold. The onset energy is thus obtained by a linear extrapolation to zero emission signal.

The experimental threshold energy E'_{thr} and the energy defect ΔE for several O I transitions are compared in Table IV; in all cases except the $3p'\,^1F \rightarrow 3s'\,^1D^0$ transition, they differ by a few tenths of an eV. Several studies of vuv emission from the photodissociation products of O_2 have shown a sharp increase in the production of

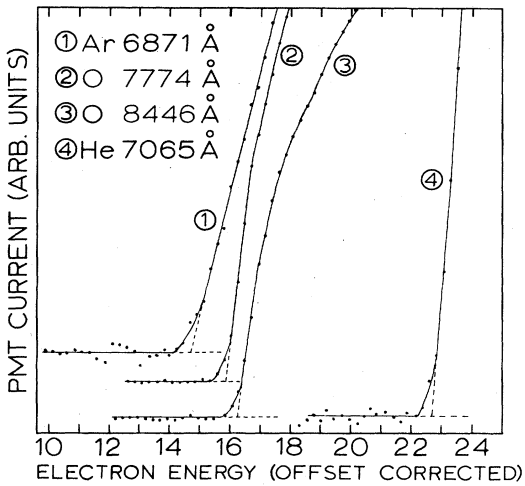

FIG. 8. Experimental signal resulting from the electron-energy distribution function convoluted with the onset of the cross-section curves for 7774- and 8446-Å O I emission. The experimental threshold accelerating voltage is obtained by an extrapolation of the steeply rising curve to zero emission signal. The threshold of the comparison He or Ar transition establishes a known point on the electron-energy axis.

$3s\,^3S^0 \rightarrow 2p^4\,^3P$ radiation at an incident photon energy of 16.1 eV.[26–28] This corresponds to the threshold production of $O(3p\,^3P)+O(2p^4\,^3P)$ and the subsequent $3p\,^3P \rightarrow 3s\,^3S^0$ cascade, in agreement with our measured onset for this process. Carlson[27] also observed photodissociative excitation of the 7774-Å multiplet with a threshold photon energy of 15.9 eV, which agrees with our result.

IV. DISCUSSION

A. Cross sections and excitation functions

The excited states of O which lie below the first ionization limit are well described by the Russell-Saunders coupling. A configuration $2p^3nl$ comprises a number of levels characterized by L, S, and J. Only in a few cases were we able to resolve the fine structure ($J' \rightarrow J$) of a multiplet. Thus the optical cross sections reported in Table I of this paper correspond to the sum of the intensities of *all* the $J' \rightarrow J$ components within a given $L'S \rightarrow LS$ multiplet transition, except where noted. Coupling the $2p^3(^4S^0)$ ground state of the O^+ ion with an outer electron (nl) results in a triplet or quintet state of the O atom. The singlet states and some triplet states are associated with parent ions $O^+(^2D^0)$ and $O^+(^2P^0)$, and thus have higher energies than the corresponding states with the $O^+(^4S^0)$ core. Many of the states which lie above the first ionization limit deviate from pure LS coupling, giving rise to several strong intercombinations between singlet and triplet levels. The intensities of transitions from these high-lying levels may also be influenced by varying degrees of au-

TABLE II. Excitation cross sections for O emission in the visible and near-infrared region, as determined by other researchers.

O multiplet	λ (Å)	Cross section (10^{-20} cm^2) This work	Other researchers	Incident electron energy (eV)
$3p\,^3P \rightarrow 3s\,^3S^0$	8446	200±30	200±30[a]	100
			230[b]	
$4p\,^3P \rightarrow 3s\,^3S^0$	4368	3.6±0.7[c]	4.7±0.7[a]	83
$3d\,^3D^0 \rightarrow 3p\,^3P$	11 287	52±10	50[b]	100
$3s'\,^3D^0 \rightarrow 3p\,^3P$	7982–7987	<0.10±0.02	<0.1[b]	100
	7995		<0.0048[d]	
$3p'\,^3D_{3,2} \rightarrow 3s'\,^3D^0_3$	8222	4.2±0.6	4.7[d]	100
$4s\,^5S^0 \rightarrow 3p\,^5P$	11 299	61±12	50[b]	100
$3p\,^5P \rightarrow 3s\,^5S^0$	7774	430±64	480[b]	100
$5d\,^5D^0 \rightarrow 3p\,^5P$	5330	2.1±0.3[e]	2.0[f]	300

[a]Reference 4.

[b]Reference 11. Experimental uncertainty limits not given in Ref. 11.

[c]Our absolute measurement given in Table I is made at 50 eV in order to eliminate the signal from the overlapping O^+ lines $3d\,^2D_{3/2} \rightarrow 3p\,^2D^0_{3/2}$ (4369.28 Å) and $3p\,^4P^0_{3/2} \rightarrow 3s\,^4P_{5/2}$ (4366.90 Å). At 83 eV most of the ion signal could be identified and subtracted away; this was done to obtain a more accurate result.

[d]Reference 15. Cross sections relative to that of the 8446-Å line, taken as 220×10^{-20} cm^2. Experimental uncertainty limits not given in Ref. 15.

[e]Measured at $p=8.0$ mTorr. We estimate that the nonlinear dependence of emission signal on pressure is negligible at 8 mTorr for $E=300$ eV.

[f]From Fig. 2 of Ref. 14. Experimental uncertainty limits not given in Ref. 14.

toionization.

All the excitation curves in Fig. 7 have a broad peak at 90—100 eV with a shoulderlike structure of varying degree near 35 eV. This feature was also found in dissociative excitation of N_2. To exhibit the shoulder structure between 35 and 45 eV more clearly, we show in Fig. 9 excitation functions for four transitions over the energy range 0—200 eV. Analogous to the case for nitrogen, we attribute the part of the excitation function below 35 eV to

$$O_2 \xrightarrow{e^-} O_2^* \rightarrow O(2p^4\,{}^3P) + O(2p^3\,nl), \quad n = 3,4,\ldots \tag{3}$$

and the broad peak to dissociation through the molecular ion, i.e.,

$$\begin{aligned} &O_2 \xrightarrow{e^-} O_2^{+*} + e^- , \\ &O_2^{+*} \rightarrow O^+(2p^3) + O(2p^3\,nl), \quad n = 3,4,\ldots . \end{aligned} \tag{4}$$

For the transitions studied in this work, process (3) has an energy defect ΔE in the range 15.8—21.5 eV ($n \geq 3$), whereas in the case of process (4) with O^+ in the $^4S^0$ state, the energy defect is 29.5—35.1 eV. These values are consistent with the onsets of the narrow peak (shoulder) and the broad maximum in the excitation function if we regard the observed $O(2p^3\,nl)$ emission as due to both processes (3) and (4). Our identification of process (4) with the onset of the broad maximum is consistent with the results of the O_2 photodissociation experiment of Lee *et al.*[28] They observed a sharp increase in the cross section for O I 1152- and 1218-Å fluorescence for incident photon energies slightly above the energetic onset for dissociative ionization. The broad maximum is characteristic of simultaneous ionization and excitation like the first step of process (4). For comparison we show in Fig. 10 the excitation function for the 4650-Å line of the atomic oxygen ion, i.e., $O^+(2p^2 3p\,{}^4D^0) \rightarrow O^+(2p^2 3s\,{}^4P)$, which results from the simultaneous ionization and excitation process

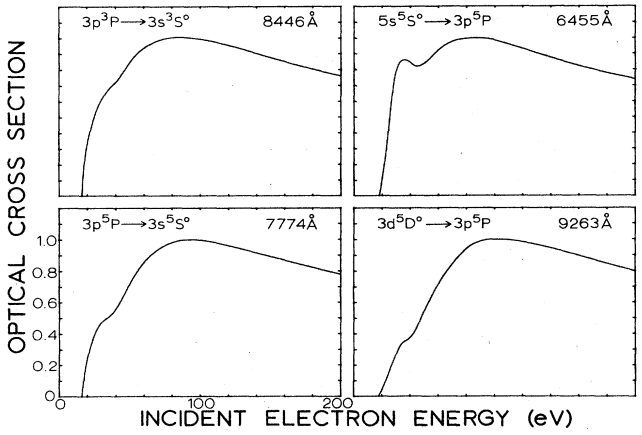

FIG. 9. Representative optical-emission excitation-function shapes for atomic-oxygen multiplet radiation in the (0—200)-eV incident-electron-energy range. The experimental data for each curve have been normalized to a maximum value of 1.0. The shoulderlike structure near 35 eV is clearly displayed in this expanded energy scale.

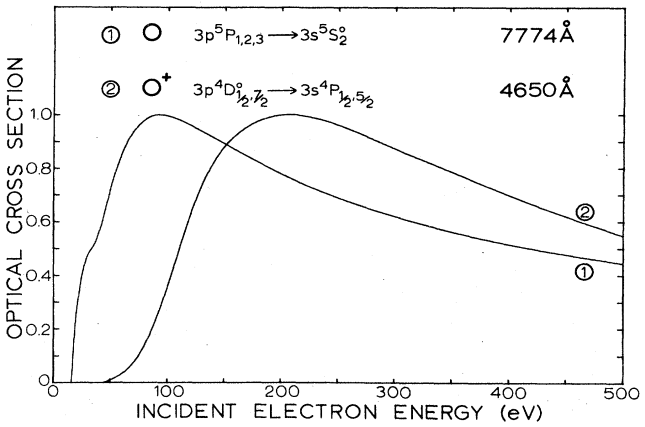

FIG. 10. Comparison of optical-emission excitation-function shape for (1) $3p\,{}^5P_{1,2,3} \rightarrow 3s\,{}^5S^0_2$ (7774 Å) of O, and (2) $3p\,{}^4D^0_{1/2,7/2} \rightarrow 3s\,{}^4P_{1/2,5/2}$ (4650 Å) of O^+. The peak cross sections are 430×10^{-20} cm^2±15% and 17×10^{-20} cm^2±15%, respectively.

$$\begin{aligned} &O_2 \xrightarrow{e^-} O_2^{+*} + e^- , \\ &O_2^{+*} \rightarrow O^+(2p^2 3p\,{}^4D^0) + O , \end{aligned} \tag{5}$$

with an energy defect of 44.4 eV. The similarity in the shape of the major peak between the excitation functions for the neutral O atom and for the O^+ ion is evident.

It is interesting to compare our results with the optical-emission excitation functions of O I emission lines in the vuv region presented in Refs. 11 and 12. In those investigations the $3s'\,{}^3D^0 \rightarrow 2p\,{}^3P$ (λ=989 Å) and $3d\,{}^3D^0 \rightarrow 2p\,{}^3P$ (λ=1027 Å) multiplets were produced by electron-impact dissociative excitation of O_2. Both excita- is consistent with our results. The authors of Ref. 12 point out possible small breaks in the slope of these functions near 40 eV. This is similar to the $4d\,{}^3D^0 \rightarrow 3p\,{}^3P$ excitation function presented in this work. In Ref. 7 the measured excitation function of the $3s\,{}^3S^0 \rightarrow 2p^4\,{}^3P$ (λ=1305 Å) line is shown. An abrupt

TABLE III. Vacuum-ultraviolet and infrared transitions of O produced by electron impact on O_2, for which cross sections and/or excitation functions have been determined by other researchers.

Observed multiplet	λ (Å)	References
$3s''\,{}^3P^0 \rightarrow 2p^4\,{}^3P$	879	13
$3s'\,{}^3D^0 \rightarrow 2p^4\,{}^3P$	989	11,13
$3s''\,{}^1P^0 \rightarrow 2p^4\,{}^1D$	999	13
$3d\,{}^3D^0 \rightarrow 2p^4\,{}^3P$	1027	11,13
$4s\,{}^3S^0 \rightarrow 2p^4\,{}^3P$	1040	11,13
$3s'\,{}^1D^0 \rightarrow 2p^4\,{}^1D$	1152	13
$3s''\,{}^1P^0 \rightarrow 2p^4\,{}^1S$	1218	7
$3s\,{}^3S^0 \rightarrow 2p^4\,{}^3P$	1305	4,5,6,7,11
$3s\,{}^5S^0 \rightarrow 2p^4\,{}^3P$	1357	5,8,9,10
Emission lines	862—1305	12
$4s\,{}^3S^0 \rightarrow 3p\,{}^3P$	13 164	11

TABLE IV. Comparison of experimental threshold incident electron energy E'_{thr} (eV) for production of O multiplet radiation with the corresponding energy defect ΔE (eV).

O multiplet	λ (Å)	Energy defect[a] ΔE (eV)	Experimental threshold E'_{thr} (eV)	$E'_{thr}-\Delta E$ (eV)	Comparison transition[b]
$3p\,^3P\rightarrow 3s\,^3S^0$	8446	16.07	16.3±0.3	0.23±0.3	1
$4p\,^3P\rightarrow 3s\,^3S^0$	4368	17.44	18.0±0.3	0.56±0.3	3
$4d\,^3D^0\rightarrow 3p\,^3P$	7002	17.84	18.0±0.7	0.16±0.7	4
$5s\,^5S^0\rightarrow 3p\,^5P$	6455	17.74	18.6±0.4	0.86±0.4	3
$3p\,^5P\rightarrow 3s\,^5S^0$	7774	15.82	16.1±0.3	0.28±0.3	1,5
$3d\,^5D^0\rightarrow 3p\,^5P$	9263	17.16	17.6±0.3	0.44±0.3	2
$4d\,^5D^0\rightarrow 3p\,^5P$	6157	17.83	18.0±0.3	0.17±0.3	3
$5d\,^5D^0\rightarrow 3p\,^5P$	5330	18.14	18.6±0.3	0.46±0.3	3
$3p'\,^1F\rightarrow 3s'\,^1D^0$	8820	19.21	20.9±0.5	1.69±0.5	5
$3p'\,^3D_{3,2}\rightarrow 3s'\,^3D^0_3$	8222	19.13	19.3±0.6	0.17±0.6	5

[a]Sum of upper O-state energy relative to the $2p^4\,^3P_2$ ground state and the dissociation energy of the $O_2(X^3\Sigma_g^-)$ state (5.08 eV). O-state energy taken from Ref. 21.

[b]Comparison transitions, with wavelengths and onset energies (see text): (1) Ar $4d(\frac{1}{2})^0\rightarrow 4p(\frac{1}{2})$, 6871 Å, 14.71 eV; (2) He $2p\,^3P^0\rightarrow 2s\,^3S$, 10 830 Å, 20.96 eV; (3) He $3p\,^3P^0\rightarrow 2s\,^3S$, 3889 Å, 23.01 eV; (4) He $3s\,^1S\rightarrow 2p\,^1P^0$, 7281 Å, 22.92 eV; (5) He $3s\,^3S\rightarrow 2p^3P^0$, 7065 Å, 22.72 eV.

change in the curvature of the function at about 40 eV is apparent, with a shape similar to our $6s\,^3S^0\rightarrow 3p\,^3P$ function. These observations, along with a comparison of the curves in Fig. 7, strongly suggest that the excitation functions of different levels of the same series have very similar shapes. We also note that our O^+ excitation function in Fig. 10 closely resembles that of the 539-Å O^+ multiplet presented in Ref. 12.

B. Molecular dissociation near threshold

As discussed in Ref. 2, production of excited O atoms by electron impact on O_2 molecules may proceed through excitation to either a totally repulsive electronic state (α) or a partly bound state (β) as shown in Fig. 11. The threshold energy E'_{thr} for production of O* is substantially larger than the energy defect ΔE if the molecule is excited to the α state, but is nearly equal to the energy defect when the intermediate state is β, provided that the junction between the attractive part and the repulsive part of the energy curve for β is within the Franck-Condon region (defined by the classically allowed range of R_{00}) of the ground-state electronic-vibrational level. Predissociation of a bound Rydberg molecular state via coupling to a repulsive state is a third mechanism to be considered. Comparison of E'_{thr} with ΔE for some typical O I lines is shown in Table IV; they differ by a few tenths of an eV for threshold production of the O* states with the $O^+(2p^3\,^4S^0)$ core. Similarly, Ajello and Franklin[12] found $E'_{thr}-\Delta E=0.76\pm1.0$ eV for production of $3d\,^3D^0\rightarrow 2p^4\,^3P$ emission by electron impact on O_2. Thus near threshold we conclude that excitation of O_2 to states like β contributes to production of Rydberg O* states with the $O^+(^4S^0)$ core. In Ref. 2, E'_{thr} and ΔE are also found to be very close for dissociative excitation of N_2 to N* levels having the ground-state ion core. In that work the β-type states were identified as the Rydberg states associated with the $N_2^+(D^2\Pi_g)$ core. At higher incident electron energies, excitation to β-type states and to other states converging to the same dissociation limit contributes to the observed cross sections.

We have also measured E'_{thr} for transitions from two O* levels having the $O^+(^2D^0)$ core (λ=8222 and 8820 Å). Ajello and Franklin[12] report $E'_{thr}-\Delta E=0.3\pm1.0$ eV for production of O I $3s'\,^3D^0\rightarrow 2p^4\,^3P$ emission. Similarly, the cross section for production of O I $3s'\,^1D^0\rightarrow 2p^4\,^1D$ fluorescence by photodissociation of O_2 presented by Lee *et al.*,[28] shows a threshold photon energy of ~18.64 eV, corresponding to $E'_{thr}-\Delta E\simeq 0.83$ eV. Our results and those which we have cited indicate that threshold production of O* states with the $O^+(^2D^0)$ core by electron impact on O_2 also proceeds through excitation to O_2 states which are very nearly of the type β.

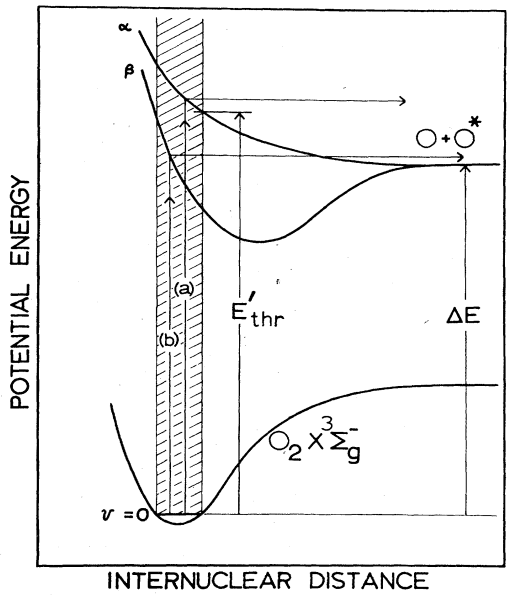

FIG. 11. Schematic representation of electron-impact dissociation process.

Extensive calculations of all O_2^+ potential-energy curves which lead to the lowest dissociation limit $O(2p^4\,^3P)+O^+(2p^3\,^4S^0)$ have been presented by Marian *et al.*,[3] along with many potential-energy curves which lead to the higher dissociation products $O(2p^4\,^3P)+O^+(2p^3\,^2D^0)$. By considering those curves for which the boundary of the continuum can be reached within the Franck-Condon region, a few states can be singled out which are likely to be most important in the threshold dissociation process leading to the production of O* with the $O^+(^4S^0)$ or $O^+(^2D^0)$ core. These are the $A^2\Pi_u$ and $b^4\Sigma_g^-$ (predissociated via $^4\Sigma_g^+$) states in the first case, and the $^2\Pi_u$(III) state in the second case. These potential curves are shown in Fig. 12. The true potential-energy curves for the dissociating system are obtained by shifting the O_2^+ curves *down* by the binding energy E_{nl} of the Rydberg electron.[2] If $O^+(2p^3\,^4S^0)$ is the atomic core, the binding energy is measured with respect to the 13.617-eV first ionization potential. If $O^+(2p^3\,^2D^0)$ is the core, the binding energy is measured with respect to the 16.947-eV ionization energy. Two examples are presented in Fig. 12.

In the case of threshold dissociation to $O(2p^4\,^3P)$ and any of the O* levels with the $2p^3\,^4S^0$ ion core, two threshold dissociation mechanisms can be found. The only β-type state which can be identified is the $A^2\Pi_u$ state. In addition, the bound $b^4\Sigma_g^-$ state is predissociated starting at $v=4$ by the $^4\Sigma_g^+$ state via spin-orbit coupling.[3] The continuum boundary of the $A^2\Pi_u$ state and the $v=4$ level of the $b^4\Sigma_g^-$ state lie at $\sim$18.7 eV above the O_2 ground state. We note that for photoproduction of O^+ from O_2 via

$$O_2 \xrightarrow{h\nu} O_2^+ \rightarrow O^+ + O\ ,$$

Dehmer and Chupka[29] found an experimental threshold of $\sim$18.7 eV ($\approx$663 Å). This coincides with the energy defect of 18.7 eV for the dissociation products

$$O^+[2p^3(^4S^0)]+O[2p^4(^3P)]$$

of the O_2^+ $A^2\Pi_u$ state. Assuming that O^+ is indeed produced at threshold via the $A^2\Pi_u$ state, this measurement indicates that it is a good example of a β-type curve. At only 0.15 eV higher, the $b^4\Sigma_g^-$ state is also predissociated by the $f^4\Pi_g$ state starting at $v=5$.

Consider production of O* in the $4d\,^5D^0$ excited level, leading to the observed $4d\,^5D^0 \rightarrow 3p\,^5P$ (6157 Å) radiation. The binding energy of the upper excited level is 0.867 eV with respect to the 13.617-eV ionization limit. The potential-energy curves of the Rydberg excited molecule are obtained by making a downward transposition of the O_2^+ curves by the amount $E_{nl}=0.867$ eV, as indicated in Fig. 12. The $A^2\Pi_u$ continuum boundary and the $b^4\Sigma_g^-$ $v=4$ level are then within the Franck-Condon region and lie at about 17.8 eV, which is in agreement with the measured onset value 18.0±0.3 eV. For the lower-lying excited atomic levels studied, these potential-energy curves for (O_2^+ + excited e^-) actually consist of several curves of different angular momentum and spin, but we still expect some of these states to be of the type β and/or predissociating states, since $E'_{\rm thr} \simeq \Delta E$ for these lower-lying levels.

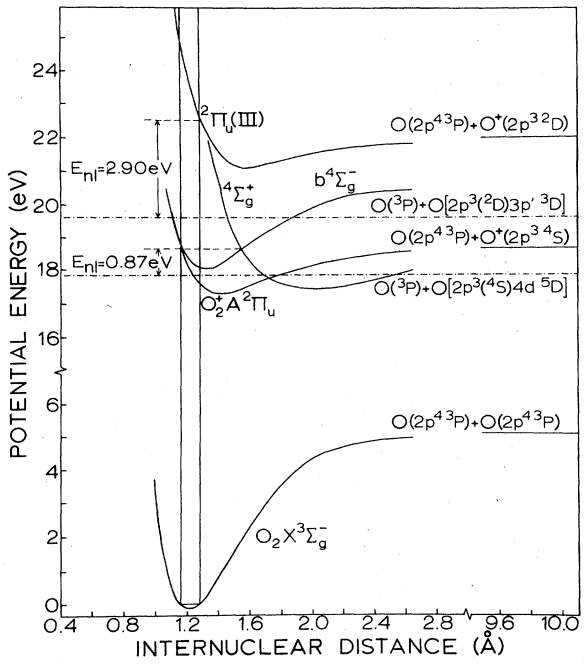

FIG. 12. Possible states of O_2^+ leading to threshold dissociation to the limits $O(2p^4\,^3P)+O^+(2p^3\,^4S)$ and $O(2p^4\,^3P)+O^+(2p^3\,^2D)$. The O^+ configuration refers to the core of the excited Rydberg O atom produced at the threshold incident electron energy for the process $O_2 \xrightarrow{e^-} O_2^* \rightarrow O(2p^4\,^3P)+O(2p^3nl)$. The true potential-energy curves for the dissociating O_2^* system are obtained by shifting the O_2^+ curves down by the small binding energy E_{nl} of the Rydberg electron (see Ref. 2). Threshold production of $O(2p^4\,^3P)+O[2p^3(^4S)4d\,^5D]$ ($E_{nl}=0.87$ eV) and $O(2p^4\,^3P)+O[2p^3(^2D)3p'\,^3D]$ ($E_{nl}=2.90$ eV) is considered here. The Franck-Condon region is indicated by the vertical lines. The O_2^+ curves are taken from Ref. 3.

In the case of threshold dissociation to $O(2p^4\,^3P)$ and any of the O* levels with the $2p^3\,^2D^0$ ion core, the lowest-lying state through which the molecule could dissociate is the $^2\Pi_u$(III) state, which is shown as the uppermost potential curve in Fig. 12. Lying only a few tenths of an eV higher are the $^4\Delta_u$(II) and $^4\Sigma_u^+$(II) states, which have nearly the same shape in the Franck-Condon region as the $^2\Pi_u$(III) state. The $^2\Sigma_u^-$ state may also be of this type, but Marian *et al.* do not extend the calculated curve into the Franck-Condon region. As a second example we now consider production of O* in the $3p'\,^3D$ excited level, leading to production of the observed $3p'\,^3D \rightarrow 3s'\,^3D^0$ (8222–8235 Å) emission. The binding energy of the upper level is $E_{nl}=2.897$ eV with respect to the first ionization limit of the $O^+(2p^3\,^2D^0)$ core. In the figure we show that when the intersection of the $^2\Pi_u$(III) state with the Franck-Condon region is shifted downward by this amount, it then lies at about 19.7 eV, which agrees with the experimental onset at 19.3±0.6 eV. Here the boundary of the continuum is slightly outside the Franck-Condon region. If a classical picture is adopted for the molecular vibration, vertical electronic excitation from the $X^3\Sigma_g^-$ ground state is completely confined within the

Franck-Condon region in Fig. 12. This would result in a minimum excitation energy of 19.7 eV. However, because the vibrational wave function extends beyond the Franck-Condon boundaries, it is possible to reach this Rydberg potential-energy curve with an incident-electron energy slightly below 19.7 eV. The experimental onset indeed is found to be 19.3±0.6 eV. Within a very small energy range above the onset, the amplitude of the vibrational wave function outside the Franck-Condon region is responsible for the dissociative excitation. This is reflected in the shape of the excitation function of the $3p'\,^3D \rightarrow 3s'\,^3D^0$ emission shown in Fig. 7; at the onset the excitation function rises very gradually with increasing incident electron energy, revealing a qualitative resemblance to the shape of the probability cloud of a harmonic oscillator outside the classical region. Here the contrast with the example of the excitation of $4d\,^5D^0 \rightarrow 3p\,^5P$ (6157 Å) radiation discussed in the preceding paragraph is especially interesting. Returning to Fig. 12, the production of O* in the $4d\,^5D^0$ level near threshold is associated with the lower curves for which the boundary of the continuum can be reached within the Franck-Condon region, unlike the $^2\Pi_u$(III) curve. Thus the portion of the vibrational wave function outside the classical region is not relevant for near-threshold dissociation. Consequently, the observed excitation function for the $4d\,^5D^0 \rightarrow 3p\,^5P$ emission shows a much more abrupt rise at threshold than that of $3p'\,^3D \rightarrow 3s'\,^3D^0$ (Fig. 7).

C. Cascade analysis of quintet transitions

For many atoms, the maximum optical-emission cross sections $Q_{\max}$ for transitions from a set of levels with given L,S to a given lower level follow the relation $Q_{\max} \propto n^{-\alpha}$, where α is a constant. The apparent cross sections for transitions from lower-lying excited states will deviate from this relation if they contain a large cascade contribution. For the $nd\,^5D^0 \rightarrow 3p\,^5P$ and $ns\,^5S^0 \rightarrow 3p\,^5P$ transitions we have sufficient data for a meaningful study of this property for oxygen. By constructing a log-log plot of $Q_{\max}$ versus n for the $nd\,^5D^0 \rightarrow 3p\,^5P$ set of transitions, we find that $Q_{\max} \propto n^{-\alpha}$ for $n \geq 4$, where $Q_{\max}$ is taken from Table I. From the least-squares-fitted curve, we find $\alpha(nd\,^5D^0 \rightarrow 3p\,^5P) = 5.258 \pm 0.002$ $(n \geq 4)$. This curve allows us to estimate maximum cross sections (100 eV) for transitions in this set which could not be measured because of overlapping molecular bands or O^+ lines. We estimate

$$Q_{\max}(6d\,^5D^0 \rightarrow 3p\,^5P) = 1.3 \times 10^{-20}\ \text{cm}^2 \pm 15\% \quad (4968\ \text{Å}),$$

$$Q_{\max}(8d\,^5D^0 \rightarrow 3p\,^5P) = 0.29 \times 10^{-20}\ \text{cm}^2 \pm 17\% (4654\ \text{Å}).$$

In the first case the atomic line lies in the O_2^+ first negative band, $\Delta v = -3$. In the second case our signal is contaminated by $O^+(3p^4D^0 \rightarrow 3s\,^4P)$ at 4650 Å. Our estimate for $Q_{\max}(8d\,^5D^0 \rightarrow 3p\,^5P)$ is consistent with our measured value $Q(50\ \text{eV}) = 0.25 \times 10^{-20}\ \text{cm}^2 \pm 20\%$. Analysis of the data trend of a similar least-squares fit to the $ns\,^5S^0 \rightarrow 3p\,^5P$ data indicates that the relation $Q_{\max} \propto n^{-\alpha}$ holds for $n \geq 6$. In this range we estimate that $\alpha(ns\,^5S^0 \rightarrow 3p\,^5P)$ is about 6.2, and

$$Q_{\max}(8s\,^5S^0 \rightarrow 3p\,^5P) = 0.13 \times 10^{-20}\text{cm}^2 \pm 20\% \quad (4802\ \text{Å}).$$

This line is contaminated by the O_2^+ second negative bandhead at 4803 Å. The calculated value is consistent with our experimentally determined upper limit of 0.17×10^{-20} cm^2 ±20%.

By combining these values with our measured cross sections for quintet transitions, we obtain a complete description of the cascade contribution to the $3p\,^5P$ level at 100-eV incident electron energy. This allows us to calculate a good estimate for the *direct* electron-impact dissociative-excitation cross section of the $3p\,^5P$ level:

$$\begin{aligned} Q_{\text{direct}}(3p\,^5P_{1,2,3}) = {} & Q(3p\,^5P \rightarrow 3s\,^5S^0) \\ & - \sum_{n=4}^{8} Q(ns\,^5S^0 \rightarrow 3p\,^5P) \\ & - \sum_{n=3}^{8} Q(nd\,^5D^0 \rightarrow 3p\,^5P) \\ = {} & 220 \times 10^{-20}\ \text{cm}^2 \pm 44\% \quad (100\ \text{eV}). \end{aligned}$$

We were not able to measure the entire excitation function of the $4s\,^5S^0 \rightarrow 3p\,^5P$ (11 298 Å) transition with the sensitivity of the present apparatus. If this excitation function can be obtained, it can be combined with the excitation functions obtained in this work for the other quintet transitions, along with their absolute optical-emission cross sections, to determine the absolute *direct* electron-impact excitation function of the $3p\,^5P$ level.

V. LONG-WAVE INFRARED EMISSION

The ratio of the optical-emission cross sections for two transitions which originate from the same upper level is equal to the ratio of the corresponding transition probabilities A, i.e.,

$$Q(i \rightarrow j) = \frac{A(i \rightarrow j)}{A(i \rightarrow k)} Q(i \rightarrow k). \tag{6}$$

Thus optical cross sections for the emission lines that share a common upper level with a transition listed in Table I can be determined by using the appropriate transition probabilities. Since direct measurement of emission intensity in the infrared, especially long-wave infrared, region is more difficult than in the visible and near-ultraviolet region, Eq. (6) allows us to obtain optical cross sections for infrared lines from the theoretical transition probabilities.

In this section we consider only transitions between levels with the $2p^3(^4S)nl$ configuration. Since the O^+ core is in a ^4S state, the total orbital angular momentum L of the oxygen atom is equal to l. An excited level is then designated by $nLSJ$. The transition probability between two levels may be written as[30]

$$\begin{aligned} A(n'L'SJ' \rightarrow nLSJ) = {} & \mathcal{S}(M)\mathcal{S}(L)a(n'L'S \rightarrow nLS)/(2J'+1), \quad (7) \\ a(n'L'S \rightarrow nLS) = {} & 64\pi^4\nu^3\sigma^2/3hc^3, \quad (8) \\ \sigma^2 = {} & e^2 \left| \int R_{nl}(r) r R_{n'l'}(r) r^2 dr \right|^2 \Big/ (4l_>^2 - 1), \quad (9) \end{aligned}$$

TABLE V. Line strength $\mathcal{S}(L)$.

	Quintets ($S=2$)			Triplets ($S=1$)		
L'-L	J'	J	$\mathcal{S}(L)$	J'	J	$\mathcal{S}(L)$
S-P	2	3	$\frac{7}{15}$	1	2	$\frac{5}{9}$
	2	2	$\frac{1}{3}$	1	1	$\frac{1}{3}$
	2	1	$\frac{1}{5}$	1	0	$\frac{1}{9}$
P-D	3	4	$\frac{9}{25}$	2	3	$\frac{7}{15}$
	3	3	$\frac{7}{75}$	2	2	$\frac{1}{12}$
	3	2	$\frac{1}{75}$	2	1	$\frac{1}{180}$
	2	3	$\frac{14}{75}$	1	2	$\frac{1}{4}$
	2	2	$\frac{7}{60}$	1	1	$\frac{1}{12}$
	2	1	$\frac{3}{100}$	0	1	$\frac{1}{9}$
	1	2	$\frac{7}{100}$			
	1	1	$\frac{9}{100}$			
	1	0	$\frac{1}{25}$			
D-F	4	5	$\frac{11}{35}$	3	4	$\frac{3}{7}$
	4	4	$\frac{3}{70}$	3	3	$\frac{1}{27}$
	4	3	$\frac{1}{350}$	3	2	$\frac{1}{945}$
	3	4	$\frac{3}{14}$	2	3	$\frac{8}{27}$
	3	3	$\frac{3}{50}$	2	2	$\frac{1}{27}$
	3	2	$\frac{1}{175}$	1	2	$\frac{1}{5}$
	2	3	$\frac{24}{175}$			
	2	2	$\frac{2}{35}$			
	2	1	$\frac{1}{175}$			
	1	2	$\frac{2}{25}$			
	1	1	$\frac{1}{25}$			
	0	1	$\frac{1}{25}$			

where $\mathcal{S}(M)$ is the multiplet strength, $\mathcal{S}(L)$ the line strength, R_{nl} the radial wave function, and $l_>$ is the greater of l and l'. Formulas for $\mathcal{S}(M)$ and $\mathcal{S}(L)$ are given in Ref. 31. For transitions between states of the type $2p^3(^4S)nl$, the values of $\mathcal{S}(M)$ are 15 for ^5S-^5P, 150 for ^5P-^5D, 525 for ^5D-^5F, 9 for ^3S-^3P, 90 for ^3P-^3D, and 315 for ^3D-^3F. The line strengths are shown in Table V.

The radial wave functions $R_{nl}(r)$ in Eq. (9) are calculated by the Hartree-Fock self-consistent-field (SCF) procedure. To simplify the calculation, the $1s$ and $2s$ orbitals of the excited oxygen atom are taken from the SCF solution of the $O(2p^4\ ^3P)$ atom, and are not varied in the iteration cycles. In Table VI we list the values of $a(n'L'S\rightarrow nLS)$ calculated from these Hartree-Fock wave functions for the transitions which are used to obtain the long-wave infrared emission cross sections according to Eq. (6). For a given configuration $2p^3(^4S)nl$, the radial wave functions for the triplet states are different from those for the quintet states because of the different exchange terms in the Fock equations. This is particularly true for the np series on account of the strong exchange interaction between the $2p$ and np orbitals. We see in Table VI that this difference in radial functions between the triplet and quintet series is reflected in the transition probabilities.

To get an indication of the accuracy of the Hartree-Fock calculation, we have computed the transition probabilities using a different method, i.e., the self-interaction-corrected form of the local-spin-density (LSD) approximation. This method has been discussed extensively in the literature,[32–35] and thus only a brief description is presented here. In the conventional LSD or the Hartree-Fock-Slater method, the exchange potential in the Fock equations for the one-electron orbitals is approximated by a local potential proportional to the cubic root of the electron density (or spin density for spin-polarized cases) $\rho^{1/3}$. This local-exchange approximation greatly simplifies the computational work, but has a serious drawback related to the self-interaction in the following way. The effective potential of an electron in the Hartree-Fock theory consists of the electron-nucleus attraction, electron-electron Coulomb repulsion, and the exchange potential. The electron-electron Coulomb repulsion includes a term corresponding to the interaction of the electron with itself. This unphysical self-interaction is cancelled by an identical term in the exchange potential so that its presence has no effect. However, when the exchange potential is approximated by the local $\rho^{1/3}$ form, the cancellation of the self-interaction energy is not complete. One troublesome consequence of this incomplete cancellation is that for a

TABLE VI. $a(n'L'S \rightarrow nLS)$ as defined in Eq. (8).

O multiplet	λ (Å)	a (sec^{-1})
$6s\ ^5S \rightarrow 3p\ ^5P$	5437.45	1.288 24 (6)[a]
$6s\ ^3S \rightarrow 3p\ ^3P$	6048.06	1.051 74 (6)
$6s\ ^5S \rightarrow 5p\ ^5P$	71 779.87	5.447 47 (5)
$6s\ ^3S \rightarrow 5p\ ^3P$	77 211.17	4.490 93 (5)
$7s\ ^5S \rightarrow 3p\ ^5P$	5020.83	7.120 77 (5)
$7s\ ^5S \rightarrow 6p\ ^5P$	132 148.12	2.091 08 (5)
$4p\ ^5P \rightarrow 3s\ ^5S$	3948.57	3.504 77 (5)
$4p\ ^5P \rightarrow 3d\ ^5D$	59 773.34	4.933 82 (4)
$5d\ ^5D \rightarrow 3p\ ^5P$	5331.32	4.542 78 (5)
$5d\ ^5D \rightarrow 4f\ ^5F$	41 371.10	2.850 93 (3)
$5d\ ^5D \rightarrow 5p\ ^5P$	56 842.49	2.764 37 (5)
$7d\ ^5D \rightarrow 3p\ ^5P$	4774.37	1.179 38 (5)
$7d\ ^5D \rightarrow 5f\ ^5F$	46 907.72	1.093 55 (3)
$7d\ ^5D \rightarrow 6p\ ^5P$	56 026.60	4.037 33 (4)
$7d\ ^5D \rightarrow 6f\ ^5F$	126 850.42	1.392 41 (3)
$6f\ ^5F \rightarrow 3d\ ^5D$	10 678.77	1.570 35 (5)
$6f\ ^3F \rightarrow 3d\ ^3D$	10 756.48	1.509 84 (5)
$6f\ ^5F \rightarrow 5d\ ^5D$	71 440.57	5.012 00 (4)
$6f\ ^3F \rightarrow 5d\ ^3D$	72 664.23	5.127 63 (4)
$7f\ ^5F \rightarrow 3d\ ^5D$	9828.63	8.865 34 (4)
$7f\ ^3F \rightarrow 3d\ ^3D$	9894.46	8.475 34 (4)
$7f\ ^5F \rightarrow 5d\ ^5D$	45 254.09	3.019 91 (4)
$7f\ ^3F \rightarrow 5d\ ^3D$	45 742.75	3.017 14 (4)
$7f\ ^5F \rightarrow 6d\ ^5D$	118 529.35	1.767 78 (4)
$7f\ ^3F \rightarrow 6d\ ^3D$	120 577.23	1.830 95 (4)

[a]Numbers in the parentheses denote the power of 10.

neutral atom the electron potential at a large distance r from the nucleus approaches zero much faster than the correct $-1/r$ dependence, resulting in an underestimation of the net attraction and hence the ionization energy. This difficulty is partly resolved by a cutoff procedure, adopted in the Herman-Skillman formulation[36] of the Hartree-Fock-Slater method, in which the local-exchange approximation is used only in the region of r between zero and a cutoff value r_0, and for $r > r_0$ the electron potential is simply set to $-1/r$. Nevertheless, this cutoff procedure does not completely remove the spurious self-interaction, although it gives the correct asymptotic potential energy.

A more fundamental way of addressing the problem of self-interaction is to remove the self-interaction terms from the total energy in the outset. This approach has recently met with great success in calculations of electronic structure of atoms,[32–34] and is often referred to as the self-interaction correction (SIC). Of special interest to us is the paper of Harrison *et al.*,[35] which demonstrates the success of the SIC-LSD approximation for calculating energies of excited states of atoms. The SIC-LSD approximation retains the computational simplicity of the Hartree-Fock-Slater approach, but provides a significant improvement over the conventional LSD approximation.

We have applied the SIC-LSD method (spin-polarized) to calculate $a(n'L'S \rightarrow nLS)$ for the quintet states,[37] and the results agree well ($\sim 10\%$) with the values obtained by the Hartree-Fock wave functions (Table VI). The agreement between the two sets of results supports the accuracy of our calculation within the Hartree-Fock framework.

Earlier works on the transition probabilities of the oxygen atom include the calculation using wave functions determined by the Hartree-Fock-Slater method (without the SIC).[38] The formulation of the Hartree-Fock-Slater method as given in Ref. 36 uses the total electron density (rather than the spin density) in the $\rho^{1/3}$ exchange term; therefore it gives the same $R_{nl}(r)$ for the quintet and triplet states of the $2p^3(^4S)nl$ configurations. Nevertheless, compared with our values of σ [Eq. (9)] of the quintet series, those of Ref. 38 are generally within a 25% range when σ^2 is greater than 1.0. For smaller values of σ^2 the discrepancy is much larger. As pointed out in Ref. 38, the integral of Eq. (9) is very sensitive to the wave functions, particularly when severe cancellation occurs between the positive and negative contributions. Thus it is not surprising to find a much larger discrepancy between the Hartree-Fock and Hartree-Fock-Slater results for the cases where σ^2 is small.

Biemont and Grevesse[39] calculated oscillator strengths for a large number of infrared lines of atomic oxygen using the Coulomb approximation.[40,41] The Coulomb approximation takes advantage of the fact that, in the usual length formula, nearly all the contribution to the dipole matrix element comes from the outer lobes of the two wave functions involved. This asymptotic part of the wave function may be computed simply with the knowledge of the Coulombic potential and the ionization energy, since the short-range potentials such as electron-exchange potential become negligible for large r. Therefore, this method is suitable for computing the dipole matrix elements between a pair of highly excited states. It follows, on the other hand, that the validity of this method may be questioned for low-lying states, and this point is discussed in Ref. 40.

The majority of the infrared lines of Ref. 39 involve highly excited states. We have compared our values of σ^2 [Eq. (9)] with those of Ref. 39 for some 140 transitions (ns, np, nd, and nf, with n up to 10). In most cases the

TABLE VII. Excitation cross sections for long-wave infrared emission of O produced by dissociative electron-impact excitation of O_2 at 100 eV.

O multiplet	λ (Å)	$\sum_{J',J} Q_{opt}(J' \rightarrow J)$ (10^{-20} cm^2)
$5d\ ^5D^0 \rightarrow 4f\ ^5F$	41 371	0.075
$7f\ ^5F \rightarrow 5d\ ^5D^0$	45 254	0.82
$7f\ ^3F \rightarrow 5d\ ^3D^0$	45 743	0.53
$7d\ ^5D^0 \rightarrow 5f\ ^5F$	46 908	0.019
$7d\ ^5D^0 \rightarrow 6p\ ^5P$	56 027	0.20
$5d\ ^5D^0 \rightarrow 5p\ ^5P$	56 842	2.1
$4p\ ^5P \rightarrow 3d\ ^5D^0$	59 773	1.6
$6f\ ^5F \rightarrow 5d\ ^5D^0$	71 441	1.4
$6s\ ^5S^0 \rightarrow 5p\ ^5P$	71 780	0.32
$6f\ ^3F \rightarrow 5d\ ^3D^0$	72 664	1.3
$6s\ ^3S^0 \rightarrow 5p\ ^3P$	77 211	0.13
$7f\ ^5F \rightarrow 6d\ ^5D^0$	118 529	0.48
$7f\ ^3F \rightarrow 6d\ ^3D^0$	120 577	0.32
$7d\ ^5D^0 \rightarrow 6f\ ^5F$	126 850	0.024
$7s\ ^5S^0 \rightarrow 6p\ ^5P$	132 148	0.085

agreement is within 25%. About ten cases occur in which the discrepancy is greater than 25%, mostly in ^3S-^3P and ^3P-^3D series.

In computing dipole matrix elements, the relative "phase" of the pair of wave functions is an important factor. The position of the outer peak of a wave function is dictated by the details of the potential in the interior region. In our Hartree-Fock calculation the triplet and quintet functions of the same nl are shifted relative to each other because of the difference in exchange-coupling coefficients. When the Coulomb approximation is used, this effect is taken into consideration to some extent through the effective quantum number n^*, but this falls short of the rigorous treatment with the result that the wave function may be shifted by an improper amount from the hydrogenic counterpart. Although the inaccuracy in the phase shift may be small in each of the wave functions, it could lead to much greater error in the dipole matrix elements where the relative phase shift of the two functions is an important factor. The discrepancy in the ^3S-^3P and ^3P-^3D series referred to in the preceding paragraph may be attributed to the inaccuracy in the phase shift in the Coulomb-approximation wave functions.

The values of $a(n'L'S \rightarrow nLS)$ in Table VI are combined with the measured optical-emission cross sections (Table I) in accordance with Eq. (6) to yield optical cross sections for a number of infrared lines. Since the individual $J' \rightarrow J$ components of an $n'L'S \rightarrow nLS$ transition are not resolved in the measured emission, we assume that the population of the J' levels (due to electron impact) within an $n'L'S$ term is proportional to the statistical weight, $2J'+1$. The optical cross sections for fifteen $n'L'S \rightarrow nLS$ transitions in the (40 000—140 000)-Å range obtained in this way are summarized in Table VII.

ACKNOWLEDGMENTS

The authors wish to thank Dr. A. R. Filippelli and Dr. R. A. Heaton for helpful advice and assistance. This work is supported by the U. S. Air Force Office of Scientific Research and by the U. S. Air Force Geophysics Laboratory.

[1]See, for example, H. S. W. Massey, E. H. S. Burhop, and H. B. Gilbody, *Electronic and Ionic Impact Phenomena* (Oxford University Press, London, 1969), Vol. II.

[2]A. R. Filippelli, F. A. Sharpton, C. C. Lin, and R. E. Murphy, J. Chem. Phys. **76**, 3597 (1982). This work reports production of N* in the configurations $2p^23p$, $2p^24p$, $2p^25p$, $2p^23d$, $2p^24d$, $2p^23p'$, and $2p^23d'$.

[3]C. M. Marian, R. Marian, S. D. Peyerimhoff, B. A. Hess, R. J. Buenker, and G. Seger, Mol. Phys. **46**, 779 (1982).

[4]G. M. Lawrence, Phys. Rev. A **2**, 397 (1970).

[5]J. M. Ajello, J. Chem. Phys. **55**, 3156 (1971).

[6]J. F. M. Aarts and F. J. DeHeer, Physica (Utrecht) **56**, 294 (1971).

[7]M. J. Mumma and E. C. Zipf, J. Chem. Phys. **55**, 1661 (1971).

[8]W. L. Borst and E. C. Zipf, Phys. Rev. A **4**, 153 (1971).

[9]R. S. Freund, J. Chem. Phys. **54**, 3125 (1971).

[10]W. C. Wells, W. L. Borst, and E. C. Zipf, Chem. Phys. Lett. **12**, 288 (1971).

[11]E. C. Zipf, R. W. McLaughlin, and M. R. Gorman, Planet. Space Sci. **27**, 719 (1979).

[12]J. M. Ajello and B. Franklin, J. Chem. Phys. **82**, 2519 (1985).

[13]H. D. Morgan and J. E. Mentall, J. Chem. Phys. **78**, 1747 (1983).

[14]V. T. Koppe, A. G. Koval, N. P. Danilevskii, and L. I. Popova, Opt. Spectrosc. **33**, 326 (1972).

[15]P. W. Erdman and E. C. Zipf, J. Geophys. Res. **88**, 7245 (1983).

[16]Electron. Technology Inc., Kearny, NJ 07032. Up to three of these filaments can be mounted in parallel to increase the electron-beam current.

[17]F. A. Sharpton, R. M. St. John, C. C. Lin, and F. E. Fajen, Phys. Rev. A **2**, 1305 (1970); F. A. Sharpton, Ph.D. thesis, University of Oklahoma, 1968.

[18]See Ref. 17. In evaluating $F(\lambda,T)$, the emissivity of tungsten $e(\lambda,T)$ was taken from L. N. Latyev, V. Ya Chekhovskoi, and E. N. Shestakov, High Temp.-High Pressures **4**, 679 (1972).

[19]B. Van Zyl, G. H. Dunn, G. Chamberlain, and D. W. O. Heddle, Phys. Rev. A **22**, 1916 (1980).

[20]A. R. Filippelli, S. Chung, and C. C. Lin, Phys. Rev. A **29**, 1709 (1984).

[21]C. E. Moore, *Selected Tables of Atomic Spectra,* Natl. Bur. Stand. (U.S.) Ref. Data Ser. No. 3 (U.S. GPO, Washington, D.C., 1976), Sec. 7.

[22]A. R. Filippelli, Ph.D. thesis, University of Wisconsin—Madison, 1984.

[23]J. Bromander, N. Durić, P. Erman, and M. Larson, Phys. Scr. **17**, 119 (1978).

[24]W. L. Weise, M. W. Smith, and B. M. Glennon, Natl. Bur. Stand. (U.S.) Ref. Data Ser. No. 4 (U.S. GPO, Washington, D.C., 1966), Vol. I.

[25]A. K. Pradhan and H. E. Saraph, J. Phys. B **10**, 3365 (1977).

[26]K. D. Beyer and K. H. Welge, J. Chem. Phys. **51**, 5323 (1969).

[27]R. W. Carlson, J. Chem. Phys. **60**, 2350 (1974).

[28]L. C. Lee, R. W. Carlson, D. L. Judge, and M. Ogawa, J. Chem. Phys. **61**, 3261 (1974).

[29]P. M. Dehmer and W. A. Chupka, J. Chem. Phys. **62**, 4525 (1975).

[30]E. U. Condon and G. H. Shortley, *The Theory of Atomic Spectra* (Cambridge University Press, London, 1963).

[31]F. Rohrlich, Astrophys. J. **129**, 441 (1959).

[32]I. Lindgren, Int. J. Quantum Chem. Symp. **5**, 411 (1971).

[33]J. P. Perdew, Chem. Phys. Lett. **64**, 127 (1979).

[34]J. P. Perdew and A. Zunger, Phys. Rev. B **23**, 5048 (1981).

[35]J. G. Harrison, R. A. Heaton, and C. C. Lin, J. Phys. B **16**, 2079 (1983).

[36]F. Herman and S. Skillman, *Atomic Structure Calculations* (Prentice-Hall, Englewood Cliffs, NJ, 1963).

[37]Application of the SIC-LSD approximation to calculate the SCF orbitals is much more difficult for the triplet states of the $2p^3(^4S)nl$ configurations since these states, unlike the quintet states, cannot be represented by a single-determinant

wave function.
[38]P. S. Kelly, J. Quant. Spectrosc. Radiat. Transfer **4**, 117 (1964).
[39]E. Biemont and N. Grevesse, At. Data Nucl. Data Tables **12**, 217 (1973).
[40]D. R. Bates and A. Damgaard, Philos. Trans. R. Soc. London **242**, 101 (1949).
[41]H. Friedrich, K. Katterbach, and E. Trefftz, J. Quant. Spectrosc. Radiat. Transfer **10**, 11 (1970).